Electronic Properties of Phenylated Ligand-Capped Nanoparticle Films

by

Thomas C. Schilling

Submitted to the Department of Materials Science and Engineering in
Partial Fulfillment of the Requirements for the Degree of

Bachelor of Science

at the

Massachusetts Institute of Technology

June 2006

Signature of Author.....
Department of Materials Science and Engineering
May 26, 2006

Certified by.....
Francesco Stellacci
Assistant Professor of Materials Science and Engineering

Accepted by.....
Caroline Ross
Chairman, Undergraduate Thesis Committee

ELECTRONIC PROPERTIES OF PHENYLATED LIGAND-CAPPED NANOPARTICLE FILMS

by

Thomas C. Schilling

Submitted to the Department of Materials Science and Engineering
on May 26, 2006 in Partial Fulfillment of the
Requirements for the Degree of Bachelor of Science in
Materials Science and Engineering

ABSTRACT

An investigation was carried out of the electronic characteristics of drop-cast films comprised of phenylated ligand-capped gold nanoparticles. In homoligand-type films, the dominant mechanism of charge transfer was expected to involve orbital overlap and end group-effected wave function displacement, whereas heteroligand-type films were expected to conduct through less efficient hopping mechanisms. Films utilizing the former mechanism are expected to have great applicability within microelectronics and rapid-prototyping technologies due to the small scale (2-6nm) of functionalized nanoparticles and the structural flexibility of interdigitation as a form of inter-particle bonding.

The comparative conductances of the cast films reveal a strong correlation with the ligand Hammaker constant (effectively a measure of the work function of the conjugated bond with the gold core of the nanoparticle and the charge displacement effected by the electronegativity or polarity of the ligand end group). The conductance was also greatly affected by the size of ligand end groups – a rough measure of the close-packing ability of a given ligand both within the ligand shell and amongst the shells of adjacent nanoparticles. The following experiments illustrate these correlations, as well as the effects of ligand spacing and shell composition on the dominant charge transfer mechanism.

Thesis Supervisor: Francesco Stellacci
Title: Assistant Professor of Materials of Science and Engineering

Table of Contents

Abstract 1

List of Figures 3

List of Tables 3

Acknowledgements 4

1. Introduction and Overview
- 1.1 Overview 5
- 1.2 Background: Phenylated Ligand Interdigitation & Conjugation 7

2. Experiment
- 2.1 Nanoparticle Synthesis
  - 2.1.1 Single-Phase Synthesis 13
  - 2.1.2 Two-Phase Synthesis 14
- 2.2 Nanoparticle Purification 16
  - 2.2.1 Soxhlet Extraction 17
- 2.3 UV-Vis Absorption Spectroscopy 18
- 2.4 Nanoparticle Film Depostion 19
- 2.5 Electronic Testing 19

3. Results and Discussion 22
- 3.1 The Effects of Phenylated Ligands 29
- 3.2 The Effects of Close-Packing 30
- 3.3 The Effects of Donor/Acceptor Level 30
- 3.4 Ligand Shell Phase Separation & Nanoparticle Morphology 32

4. Conclusions & Suggestions for Future Work 32

References 35

List of Figures

Figure 1. Illustrations of nanoparticle ligand shell morphologies **6**

Figure 2. Schematic illustration of charge transfer and interdigitation **8**

Figure 3. Schematic representations of all ligands used in study **11**

Figure 4. Single-nanoparticle I(V) curves measured on STM **12**

Figure 5. Test substrate, illustration of test pads, illustration of electrodes **20**

Figure 6. Illustration of interdigitated electrode ends **20**

Figures 7-10. Representative I(V) curves for each nanoparticle film type **23-26**

Figure 11. Plot of average conductance (high-range) for each film type **28**

Figure 12. Plot of average conductance (low-range) for each film type **28**

List of Tables

Table 1. Nanoparticle and solvent combinations **19**

Table 2. Average conductance for each type of nanoparticle film **27**

Acknowledgements

I must acknowledge and thank my thesis advisor and long-time UROP supervisor Professor Francesco Stellacci for his guidance, encouragement, and friendship throughout the past three years. His enthusiasm for my projects often sustained my interest in scientific work, and thanks to his efforts and inspiration, I will forever feel attached to the materials science community. The post-doctoral workers and graduate students in his group, most particularly Alicia Jackson, Benjamin Wunsch, Gretchen DeVries, Robert Barsotti, Xiaogang Liu, Brenda Long, Tan Mau Wu, and Jeff Kuna, have all contributed to my development as a materials scientist. My fellow UROPs, particularly Paulo Jacob-Silva and Mike Dimitriou, often assisted me with my experiments and kept me company during late-night syntheses. Working in a laboratory full of good friends and helpful colleagues has made all of my time working with Professor Stellacci feel like time well-spent.

The current study would not have been possible without the support of Professor Rafael Reif, who allowed me to use his two-point probe measurement station to test the cast films. Tan Mau Wu, a graduate student in both Professor Reif's and Professor Stellacci's groups, helped to train me on the equipment and troubleshoot problems as they arose. Tan also helped to manufacture the electrodes used in the current study – a generous favor that vastly simplified the entire experimental process. Gretchen DeVries contributed data culled from previous work on single nanoparticle experiments, and provided helpful insights throughout both the synthesis and testing stages of the project. Jeff Kuna devoted many hours to this project: he often assisted me with my syntheses, and he accompanied me on nearly every foray to Professor Reif's electronic testing lab. Furthermore, in our conversations, Jeff helped me to conceptualize the many different aspects of this project, and he even helped to edit this report. For all of these things, I am extremely grateful to Jeff and to the many people that assisted me in this study.

1. Introduction and Overview

1.1 Overview

Rapidly developing photolithographic techniques made great strides in keeping the microelectronics industry on pace with Moore's Law for the past several decades, but the physical limitations of these techniques have begun to slow the pace of feature miniaturization. Scientists have long predicted that this branch of microelectronics technology development will effectively hit a brick wall and further miniaturization (beyond the feature size range of several hundred nanometers) will become impossible [1]. Industry experts and materials scientists in academic institutions worldwide have begun work on new technologies to replace the paradigmatic set of photolithographic techniques. The possibilities (and limitations) of these new technologies are only now beginning to be understood in the context of the vast and varied technoeconomic world of integrated circuits.

Given the time, difficulty, and materials and labor cost required to produce standard integrated circuits via photolithography, many of these emergent technologies have concerned themselves with simplifying the creation process. Several major corporations have postulated that simple integrated circuits and other devices can be printed onto a variety of substrates as simply as modern day inkjet printers put ink to paper [2,3]. This would allow engineers, after making subtle modifications to currently existing inket systems, to rapidly print electronic circuits onto any material. Furthermore, chemically-modified colloidal gold is of great interest for its applicability in rapid prototyping processes, as the large surface area to volume ratio of nanoparticles makes them prime candidates for selective laser sintering [4]. The ability to use these methods

to create intricate, electronically conductive three-dimensional structures would allow engineers to vastly simplify traditional vapor deposition protocols. In order to make all of these printing processes feasible, the electronic properties of these potential "inks" must be thoroughly characterized.

The research group of Professor Francesco Stellacci has adapted a method for synthesizing gold nanoparticles capped with a wide range of organic and inorganic ligands within a size range of 2-6nm [5,6]. **Figure 1** shows illustrations of both homo- and heteroligand capped nanoparticles; the illustration of the heteroligand-capped

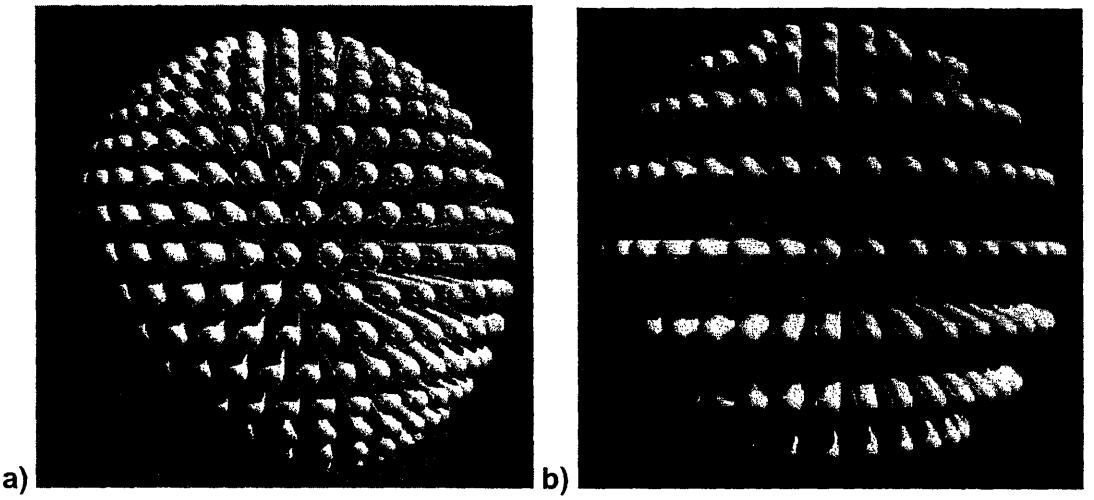

Figure 1. Illustrations of the ligand shell morphologies as shown in [7] for **a)** homo- and **b)** heteroligand-capped nanoparticles.

nanoparticle displays a rippled morphology in the ligand shell, a phenomenon demonstrated using scanning tunneling microscopy (STM) [7,8]. The possible uses of these nanoparticles extend from coatings for biomedical devices and components in biosensors to conductive layer-forming "inks" that might soon make inkjet circuit printing a viable alternative to photolithography. While non-functionalized gold

nanoparticles could indeed be deposited onto substrates and sintered together to form structurally robust circuit lines, the use of gold nanoparticles linked by heavy interdigitation (as opposed to crystalline, metallic bonds between gold atoms) would enable circuit flexibility unimaginable with current lithography technology. This benefit over normal photolithography onto solid silicon substrates would have far-reaching results for the technologies of integrated circuits. Putting circuit lines onto diverse materials is the first step towards incorporating processors into any space they might be needed. As far as miniaturization is concerned, a printing technique capable of laying lines one nanoparticle wide (a feat easily achievable via chemical functionalization of a surface) would effectively make features between 2-4 nm – a significant improvement over the 400 nm features at the cutting edge of today's integrated circuits [9].

1.2 Phenylated-Ligand Conjugation and Interdigitation

The conductivity of benzene and other phenylated molecules was first studied in the late 1960s at the beginning of scientific interest in organic semiconductors [10,11]. Pentacene in particular has aroused considerable interest within the microelectronics industry for its good conductivity and low processing temperature requirements, and it is currently used in many devices containing organic LEDs [12,13]. The electronic properties of phenylated molecules have since been studied within a wide range of contexts, ranging from nanomechanical sensory applications [14] to areas of pharmaceutical research examining charge-transfer complexes in biological processes[15]. Previous studies have utilized benzene's felicity for interdigitation in the synthesis of optical materials from phenylated molecules [16], and other studies have

introduced phenyl groups with the sole intention of increasing electronic conductivity in polymers (although not all of these processes have produced the expected effect) [17,18].

Previous attempts to assemble novel nanostructures from capped nanoparticles have often relied upon secondary chemical interactions between ligand endgroups as linkages [19]. The stability of layers formed through endgroup interactions has been investigated for hydrogen bonding groups like mercaptoundecanol [20] and Van der Waals couples like octanethiol [21]. The current study represents a diversion from these previous investigations in that it investigates chemistries designed to produce heavy interdigitation along the length of the capping ligands so as to increase both layer stability and improved electronic conductivity between the linked nanoparticles. Because of their capacity for pi-pi stacking and conjugation with the gold nanoparticle core, phenylated capping ligands were chosen for the current study.

Figure 2 illustrates the mechanisms of both charge transfer and interdigitation as

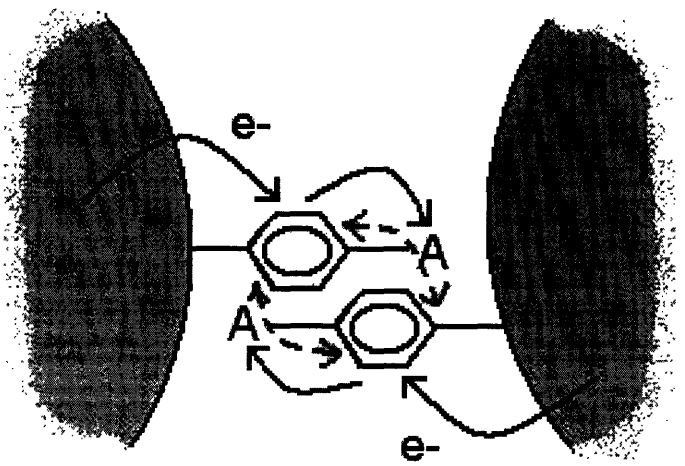

Figure 2. A schematic illustration of charge transfer and interdigitation between conjugated phenylated ligand shells of adjacent nanoparticles. The arrows connected by dotted lines represent pi-pi stacking between phenyl groups, and the solid-line arrows represent the displacement of charge away from the gold nanoparticle core (here shown as grey semi-circles) and out to the acceptor endgroups.

they would function in a film composed of interdigitated, phenylated ligand-capped nanoparticles. With sufficient close-packing between conjugated ligands, the overlapping orbitals characteristic of the phenyl groups will join with each other in a pi-pi stacking configuration, diffusing charge density throughout each ligand shells and between adjacent nanoparticles. The electron withdrawing or donating level of the ligand endgroups, often simply referred to as the Hammett constant, is determined by the electronegativity or polarity of end groups on the conjugated ligand as well as by the work function of the sulfur-gold bond tethering the phenylated ligand to the gold core. The strength of this Hammet constant effects the displacement of charge across the conjugated bonds between the phenylated ligands and the gold core, resulting in an overlapping of wavefunctions and the creation of either HOMO (highest occupied molecular orbital) or LUMO (lowest unoccupied molecular orbital) conduction states, depending on whether the Hammet constant of the capping ligand endgroup makes it a charge donor or acceptor, respectively. This electronic configuration is not unlike that produced in doped semiconductors, whereby the presence of charged impurities enables electronic conduction throughout the doped region of the semiconductor material through artificial states.

The range of phenylated ligands used in the current project allowed for the comparison of a number of different endgroup configurations in order to demonstrate the relative effects of electron acceptor/donor levels, capacity for secondary bonding, and close packing ability. Theoretically, the capping ligands best suited to interdigitation and electronic conduction between nanoparticles would have small end groups and thus be capable of extremely close packing. Such a physical configuration would minimize the

distance between the pi-stacked benzene sections of the conjugated ligands, allowing for maximum wavefunction overlap. Furthermore, endgroups with high acceptor or donor levels, such as alcohol groups and fluorine atoms, would further assist charge transfer between interdigitated ligand shells. **Figure 3** shows schematic illustrations of each of the molecules used as capping ligands in the current study. In the *Results and Discussion* section of this study, these characteristics will be further investigated in the analysis of the conductance measured for each of the nanoparticle types studied.

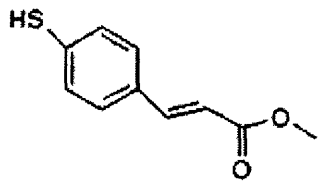

a. 4,4'-dithiobiscinnimate

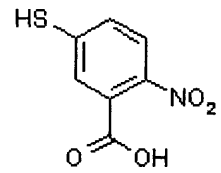

b. 5,5'-dithiobis(2-nitrobenzoic acid)

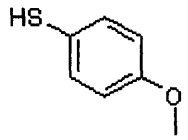

c. 4-methoxybenzenethiol

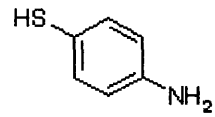

d. 4-aminophenyl disulfide

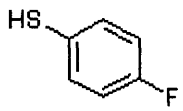

e. 4-fluorothiophenol

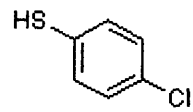

f. 4-chlorobenzenethiol

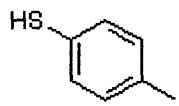

g. 4-methylbenzenthiol

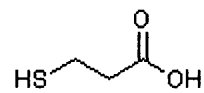

h. mercaptopropionic acid

i. octanethiol

Figure 3. Schematic representations of the ligands derived from the molecules **a)** DTBS (schematic shown of ligand post-dissociation), **b)** DTNB (post-dissociation), **c)** MoBT, **d)** APDS (post-dissociation), **e)** FTP, **f)** CBT, **g)** MBT, **h)** MPA, **i)** OT. Although nanoparticles using different homo- and heteroligand shells of all nine ligands were synthesized, only DTNB, APDS, FTP, MBT, MPA, and OT were used in the current study.

The current study seeks to further develop the findings of earlier electronic conductivity tests on phenylated ligand-capped nanoparticles in which I(V) curves were produced for single nanoparticles via STM. **Figure 4** shows the results of these tests.

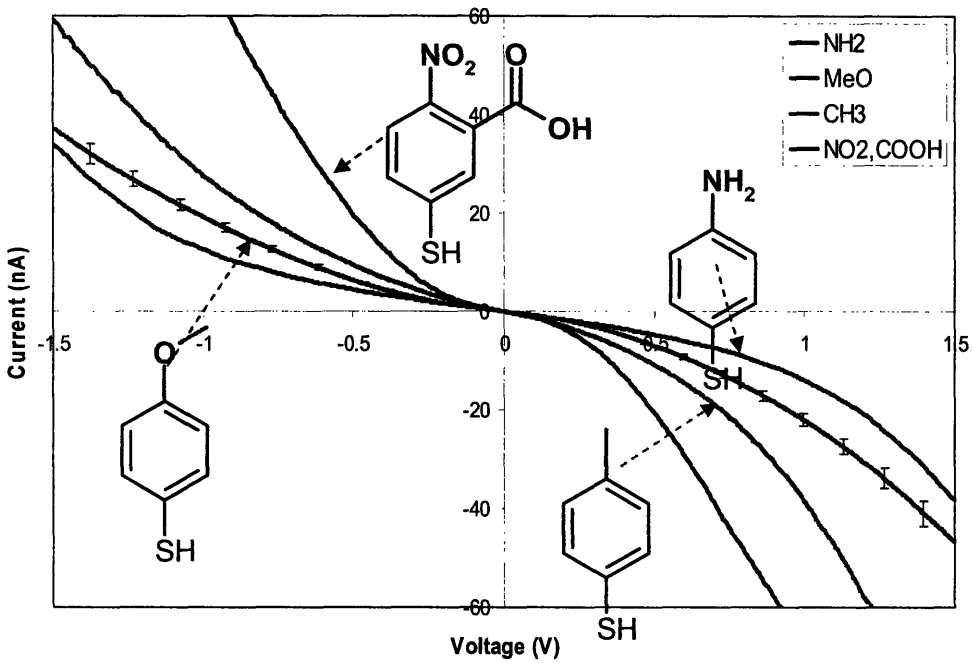

Figure 4. I(V) characteristics of single nanoparticles capped with various phenylated ligands, tested separately using STM (courtesy of Gretchen DeVries).

In order to produced I(V) curves for individual nanoparticles, an STM tip was lowered into contact with a gold surface functionalized with phenylated ligand-capped nanoparticles. As the voltage passing through the probe tip was swept between -1.5V to 1.5V, the tunneling current was measured and plotted. The resistance in these plots reflects the energetic barrier as a function of the work function of the thiol bond tethering the capping ligand to the gold core. In order to investigate the relative importance of this interaction versus the impact of morphological concerns like close-packing ability, ligand spacing, and degree of interdigitation in determining electronic conductivity, these single-

particle I(V) characteristics were compared with the I(V) characteristics of interdigitated films. In the following section, I will discuss the synthesis of the various types of nanoparticles used in the study, as well as the preparation of the test substrate, casting of the film, and the electronic testing of the film.

2. Experiment

2.1 Nanoparticle Synthesis

2.1.1 Single-Phase Reaction

Homo- and heteroligand-capped nanoparticles of a variety of ligand types were synthesized using both single-phase and two-phase reduction methods. 4-fluorothiophenol-, 4-chlorobenzenethiol-, 4-methylbenzenethiol-, 4-methoxybenzenethiol-, 5,5'-dithiobis (2-nitrobenzoic acid)-, 4-aminophenyl-disulfide-, 4,4'-dithiobiscinnimate-capped gold nanoparticles were originally synthesized via the Kang method for gold salt reduction in a single phase, albeit in a form slightly modified by the Stellacci group [5-7]. Given the extreme sensitivity of the nanoparticle nucleation process, each single-phase synthesis was performed in a round-bottom flask immersed in an ice bath to retard the kinetics of reduction. In each synthesis, 0.9mmol of gold-tetrachloroaurate ($HAuCl_4$) was dissolved in 200ml ethyl-alcohol in a 500ml round bottom flask, then left to stir for ten minutes. After the gold salt was allowed to dissolve completely, 0.9mmol of a thiolated molecule (or stoichiometric combination of thiolated molecules) was injected into the solution. At this point, the ethanol solution would

typically pass from a clear, bright yellow color to a softer, murkier yellow. Certain thiolated ligands precipitated even more dramatic color changes; as each molecule of 4-aminophenyl-disulfide dissociated into two separate ligands as it was stirred into solution with gold, the entire mixture turned bright orange.

Following this addition, the solutions were allowed to stir for 20-30 minutes. In the case of conjugated ligands like 4-aminophenyldisulfide, the time relegated to this step was increased dramatically so as to allow the molecules to dissociate into thiolated pairs. Meanwhile, the reducing agent, 1 gram of sodium borohydride ($NaBH_4$) in 200ml of ethanol, was stirred into a suspension then filtered through qualitative filter paper. After the thiolated ligands were dissociated and thoroughly stirred into the mixture, the filtered $NaBH_4$ mixture was then slowly added to the gold-thiol mixture at a rate of two drops per minute. As the reducing agent was slowly added to the gold-thiol mixture, the overall color of the mixture should change slowly from yellow to white to brown and finally to black as nanoparticles were formed. When the solution turned black, the dropping rate was increased to one drop per second. After all of the $NaBH_4$ solution was added, the mixture was stirred for several hours, then refrigerated overnight.

2.1.2 Two-Phase Reaction

Equivalent stoichiometric ratio, heteroligand combinations of octanethiol: mercaptopropionic acid-, octanethiol: 4-aminophenyl-disulfide-, and octanethiol: 4-fluorothiophenol-capped nanoparticles, as well as additional quantities of homoligand octanethiol-, 4-fluorothiophenol-, 4-methylbenzenethiol-, 5,5'-dithiobis (2-nitrobenzoic acid)-, 4-aminophenyl-disulfide-capped gold nanoparticles were produced using the two-

phase synthetic protocol, as developed by M. Brust, *et al* [5]. This method makes use of a 4-fold excess of the surfactant molecule tetraoctylammonium bromide ($BrN((CH_2)_7CH_3)_4$) (also know as TOABr) to facilitate the interfacial reaction of gold atoms and thiolated ligands and to regulate the speed of the reduction process. The protocol utilizes an identical scale as the single-phase method (0.9mmol), this time beginning with the gold salt dissolved in 50ml of deionized water. With the addition of 4mmol of TOABr in 80ml of toluene, the mixture rapidly changed from a golden to a dark red hue. The immiscibility of the water and toluene phases resulted in the formation of reverse micelles and other lamellar structures. The mixture is stirred for another 30 minutes to allow the gold salt to transfer into the organic phase, and then 0.9mmol of the ligand or combination of ligands is injected into the mixture. The mixture then stirs for another 20 minutes to give the thiolated ligands time to react with the gold ions in the aqueous phase.

The self-regulating kinetics of the interfacial reduction allow the addition of the reducing solution (0.33M solution of $NaBH_4$ sonicated into 30ml deionized water) to proceed at a slightly quicker pace. The first five to ten drops were spaced by approximately 20 seconds to limit the number of nucleation sites created, and the remainder of the solution was added at a rate of one drop per three seconds. Once all of the $NaBH_4$ solution was added, the mixture was left to stir for several hours.

The initial stages of the process used for purifying nanoparticles created with the two-phase method demand that the nanoparticles be rinsed repeatedly to remove $NaBH_4$ and TOABr before the particles can be allowed to precipitate. This is performed by pouring the nanoparticle mixture into a 500ml separation funnel, adding deionized water,

shaking the funnel, then allowing the mixture to phase-separate. Ideally, the nanoparticles would diffuse into the toluene phase, and the aqueous phase was drained off and discarded. Occasionally, some nanoparticles remained in the aqueous phase, trapped in reverse micelles.

After the nanoparticles in the toluene phase were rinsed four to five times, the solution was placed in a 500ml round-bottom flask. This flask was then rotovapped under vacuum in a water bath set to 55°C, and turned until all but 10ml of the nanoparticle solution had evaporated. The remaining toluene solution as well as the dried nanoparticles coating the inside of the flask were then brought into suspension with 400ml of ethanol and refrigerated overnight.

2.2 Nanoparticle Purification

The chemical composition of the end groups on the thiolated-ligands used in these syntheses were such that none of the created nanoparticles should have been soluble in ethanol. Consequently, the nanoparticles naturally precipitated out of the ethanol overnight. This process greatly facilitated the filtration and rinsing of the nanoparticles – a set of processes common to both single- and two-phase protocols.

After the nanoparticles were allowed to precipitate out of solution, they were filtered through quantitative filter paper set atop a Bücher funnel. The solution was then drawn through the filter paper and into a collecting flask by means of a mechanical air pump. Filtration is begun by pouring a significant volume of liquid through the filter to allow the nanoparticles and aggregates suspended in the supernatant to effectively clog the filter paper and prevent other nanoparticles from being pulled through. The entire

contents of the flask were then moved to the filter paper by means of a long pipette, and the paper surrounding the primary deposit of nanoparticles was kept wet using ethanol. Water and acetone were then used to rinse the nanoparticles deposited on the filter paper. The particles were covered to protect them from dust contamination and allowed to dry for several days, then scraped off of the filter paper and stored in a glass vial.

2.2.1 Soxhlet Extraction

The large quantity of the surfactant TOABr often resists traditional rinsing and filtration methods, leaving charged amines amongst the finished nanoparticles which can engender stronger packing and stabilization in the solid phase. This also produces misleading solubility characteristics due to dipolar interactions between the alien charged groups in the ligand shell, and solid-state electrical conductivity characteristics not representative of the nanoparticles themselves. These problems have led some groups to introduce additional steps to the purification process. Soxhlet extraction was originally employed in nanoscale material synthesis protocols for the purification of Buckminster fullerenes and nanotubes [22], and has been successfully used for removing quaternary ammonium salts remaining from two-phase nanoparticle syntheses [23]. Soxhlet extraction essentially involves the continuous rinsing of the dissolved nanoparticles by a non-compatible solvent (usually acetone or diethyl ether).

Due chiefly to time constraints, we did not employ Soxhlet extraction during our purification processes. We did, however, rinse the yield from each two phase synthesis much more vigorously and with a wider range of solvents than was characteristic of the single-phase yield rinsing processes. Although further purification steps would

undoubtedly improve the consistency and quality of the cast nanoparticle films, the wide spread of the final results from the conductivity calculations performed for each film suggest that the competing mechanisms of charge transfer made possible by presence of impurities did not have a dramatic impact upon our measurements.

2.3 UV-Vis Absorption Spectroscopy

Absorption spectroscopy has been used as a means to gauge polydispersity within specific size ranges of nanoparticle yields, as well as relative rates of agglomeration within nanoparticle solutions [24]. This is done by measuring the width and placement of the resonant frequency of the surface plasmon – a wave perturbation that arises in the electron cloud surrounding a metal nanoparticle in a solution with a positive dielectric constant when the nanoparticle is struck with a photon. The width of the peak indicates the polydispersity of the sample, and blue-shifts in the plasmon peak from the expected resonant frequency indicate agglomeration in the solution. As absorptions spectroscopy was only occasionally employed during our investigations, a detailed explanation of the process is not included in the current study.

2.4 Nanoparticle Film Deposition

Eight solutions of 4mg of dried nanoparticles in 20mL of solvent were created; the combinations used in these combinations are presented in **Table 1**.

Table 1. Nanoparticle type and solvent combinations.

Nanoparticle Type	Solvent
5,5'-dithiobis(2-nitrobenzoic acid) (DTNB)	water
4-aminophenyl disulfide (APDS)	dimethylformamide (DMF)
4-flourothiophenol (FTP)	DMF
4-methylbenzenthiol (MBT)	toluene
octanethiol (OT)	toluene
1:1 OT:FTP	toluene
1:1 OT:APDS	toluene
1:1 OT:mercaptopropionic Acid (MPA)	water

50μL of the solution containing the nanoparticle to be tested was then dropped onto a silicon substrate containing interdigitated electrodes, and the solution was allowed to evaporate at room temperature. When the substrate appeared to be completely dry, it was then placed on a hotplate and held at 60°C for 30 minutes to further evaporate the solvent and to "anneal" the deposited nanoparticle film. These steps were performed with the assumption that the polarity of the solvent used had no effect on the formation of the layer, and that in each case nanoparticles fell to the surface of the test substrate without aggregating.

2.5 Electrical Testing

After the coated substrate cooled back to near room temperature, it was placed in a two point probe electronic testing stage. The positive and negative probe tips were then visually positioned over the electrode pads via microscope, and carefully lowered onto

the pads via vertical position microadjustment dials. A picture of the patterned silicon substrate, as well as an illustration of the interdigitated electrodes is given in **Figure 5**. **Figure 6** provides a more precise schematic illustration of the interdigitated electrodes.

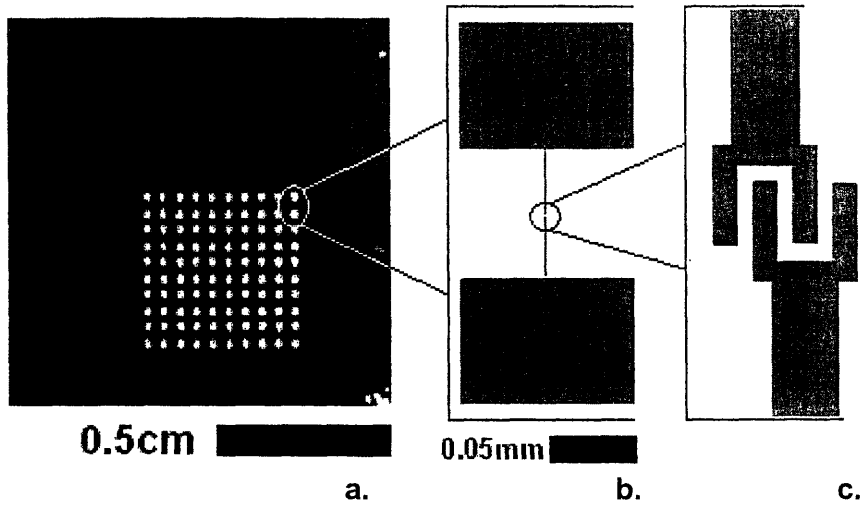

Figure 5. a) Photographic image of test substrate, **b)** high-magnification illustration showing probe tip pads of an individual interdigitated electrode, **c)** further-magnified illustration of interdigitated electrode ends.

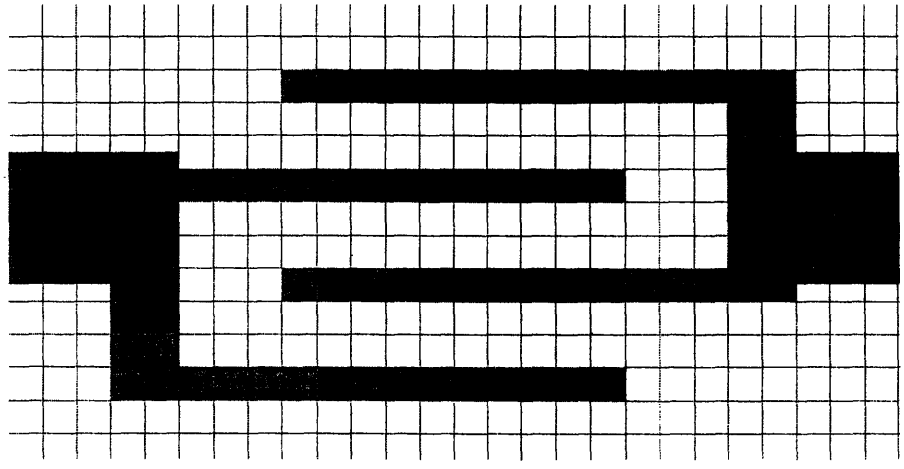

Figure 6. Schematic illustration of interdigitated electrode ends, showing approximate length scale (each square on grid represents 500nm x 500nm area).

While the electrode pads provided for probe contact measured several hundred microns on a side, the interdigitated electrodes themselves are much smaller (the finest dimension being only 500nm wide). Although the evaporation method used in our study produced nanoparticle layers of varying qualities and thicknesses, the dimensions of the electrode suggest a range of thickness between 10-100nm as none of the cast films were thick enough to visibly coat the gold surface of the electrodes. I will address the nanoparticle film variability later in this work.

Multiple IV curves were produced for each nanoparticle type using voltage and current measurements taken by an Agilent 4155C Semiconductor Parameter Analyzer. In each test, after the probes had been placed into contact with the electrodes, current measurements were taken for voltages between -100.0mV and 100.0mV, then back down to -100.0mV, in increments of 10.0mV. To account for variations in layer thickness (and during later tests, variations in electrode quality), measurements were taken from at least seven of the forty electrode pairs for each nanoparticle type, and at least three measurements were taken from each pair tested to demonstrate the stability of the electrodes. The resistances derived from each curve was then averaged together and divided by one to produce a single average value of conductance for each type of nanoparticle film.

2.6 Film Removal and Substrate Cleansing

As only two patterned substrates were available for use during our tests, a cleaning protocol was employed to remove the nanoparticle film following each round of tests. First, the coated substrate was rinsed with the solvent used to deposit the

nanoparticle film so as to begin to dissolve the layer. The substrate was then submerged into a 5:1:1 solution of water, ammonium hydroxide, and hydrogen peroxide for 30 minutes, then repeatedly rinsed with DI water and dried with compressed nitrogen gas.

3. Results and Discussion

Films of eight different types of nanoparticles were drop-cast onto a patterned silicon substrate and electronically tested to produce IV curves. These nanoparticle types included homoligand-capped gold nanoparticles capped with octanethiol, 4-fluorothiophenol, 4-methylbenzenthiol, 4-aminophenyl disulfide and 5,5'-dithiobis (2-nitrobenzoic acid),[1] and heteroligand-capped gold nanoparticles capped with 1:1 ratios of octanethiol and 4-fluorothiophenol, octanethiol and 4-aminophenyl disulfide, and finally octanethiol and mercaptopropionic acid. A set of several representative IV curves is given for each nanoparticle type in **Figures 7 - 10**.

[1] Both 4-aminophenyl disulfide and 5,5'-dithiobis (2-nitrobenzoic acid) dissociate into two separate ligands before conjugating with gold, so these chemical names refer to the chemical as it is added to the gold mixture, and not in its final conjugated state.

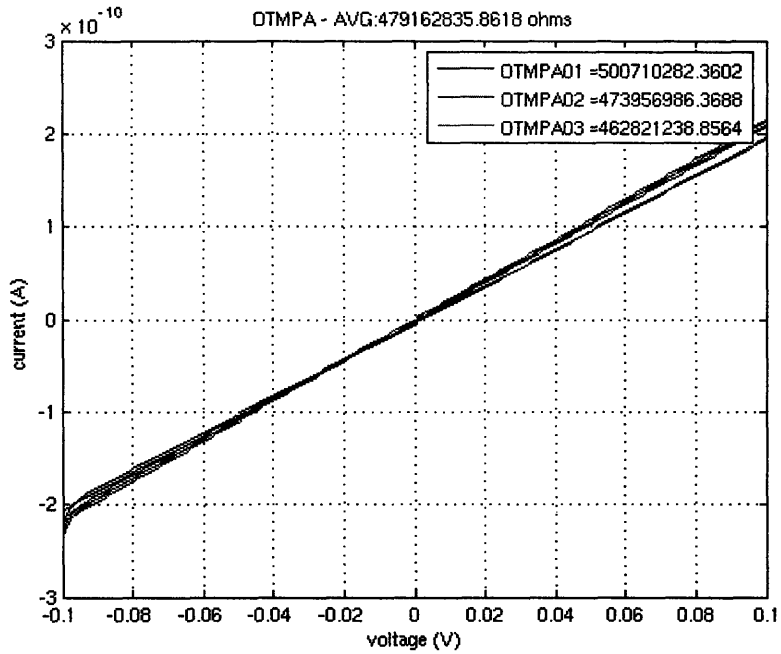

a)

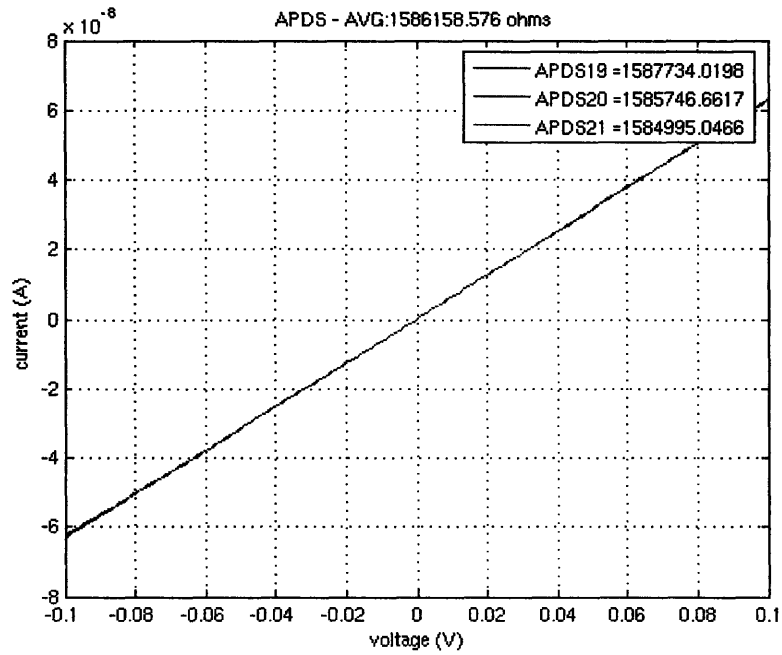

b)

Figure 7. a) A representative set of three I(V) curves measured for the film composed of OT:MPA-capped nanoparticles. The maximum measured current is outside the nanoamp range, **b)** Three I(V) curves for the APDS-type film, showing a maximum current more than two orders of magnitude greater than the OT:MPA-type film for the range of voltage used.

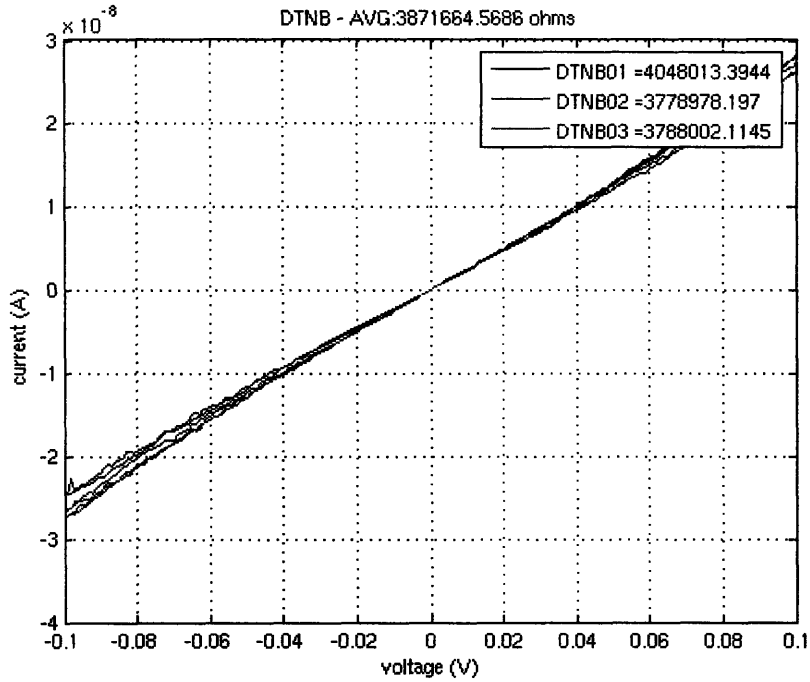

a)

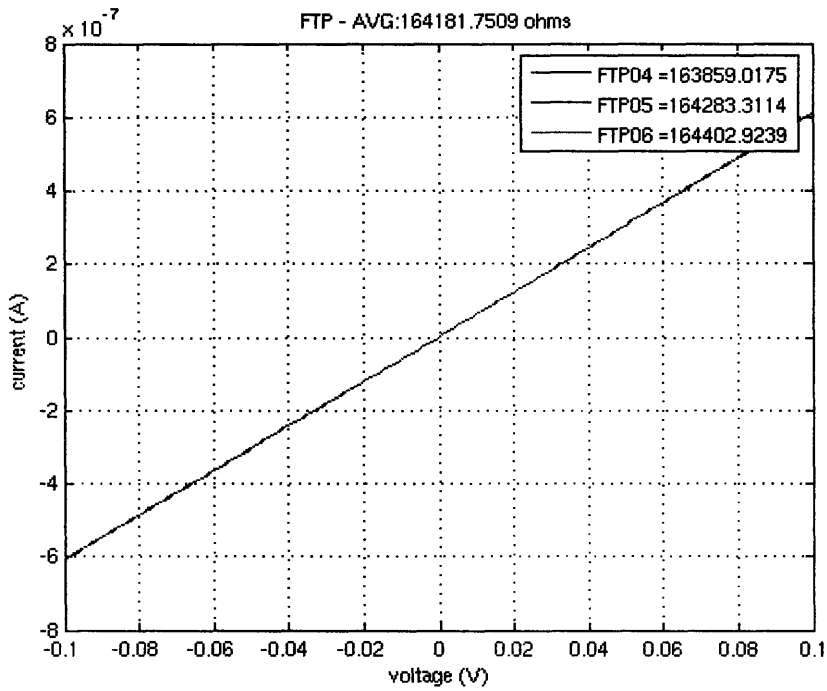

b)

Figure 8. a) Three I(V) curves measured for the DTNB-type film; subtle fluctuations in the curve at points corresponding to higher applied voltages suggest damage to the electrode **b)** Three I(V) curves for the FTP-type film, showing model I(V) behavior.

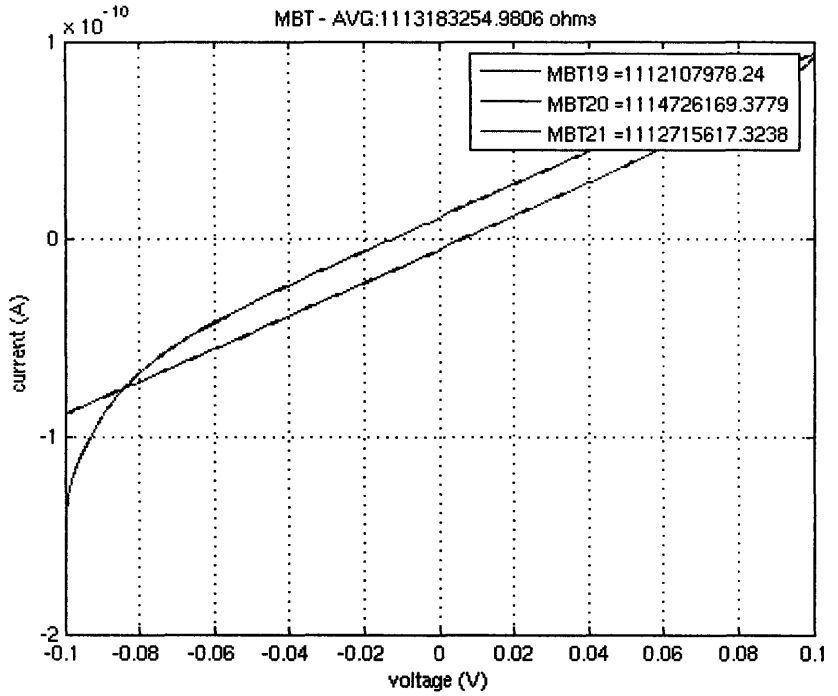

a)

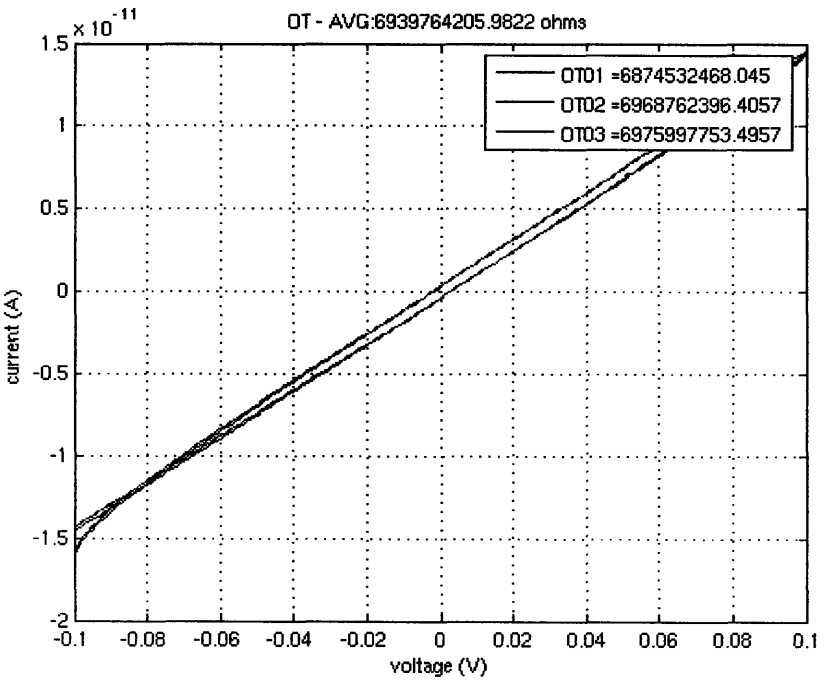

b)

Figure 9. a) Three I(V) curves for the MBT-type film, **b)** Three I(V) curves for the OT-type film, both showing substantial hysteresis, a common feature in low-current tests. In all cases, the phenomenon results from ionic conduction through unevaporated solvents.

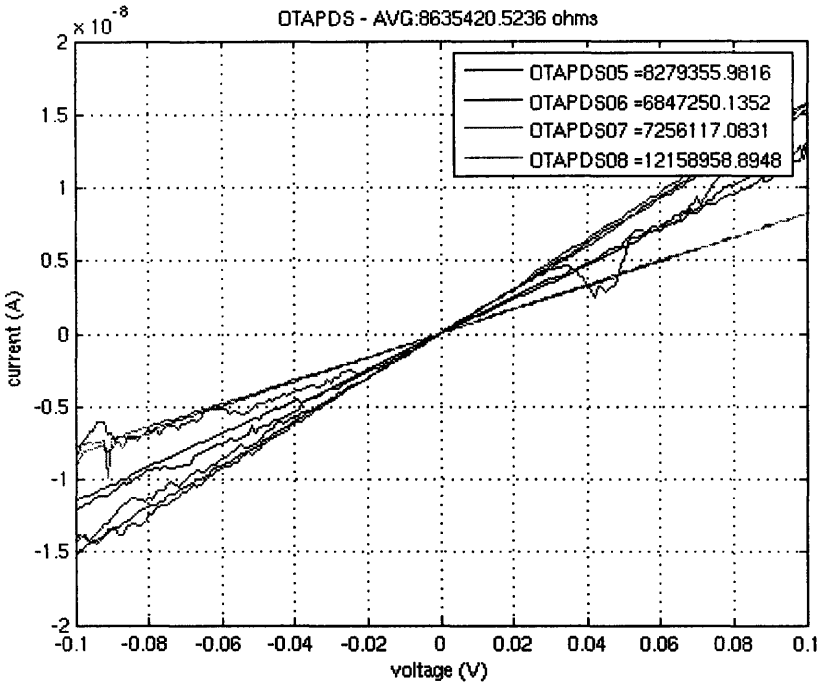

a)

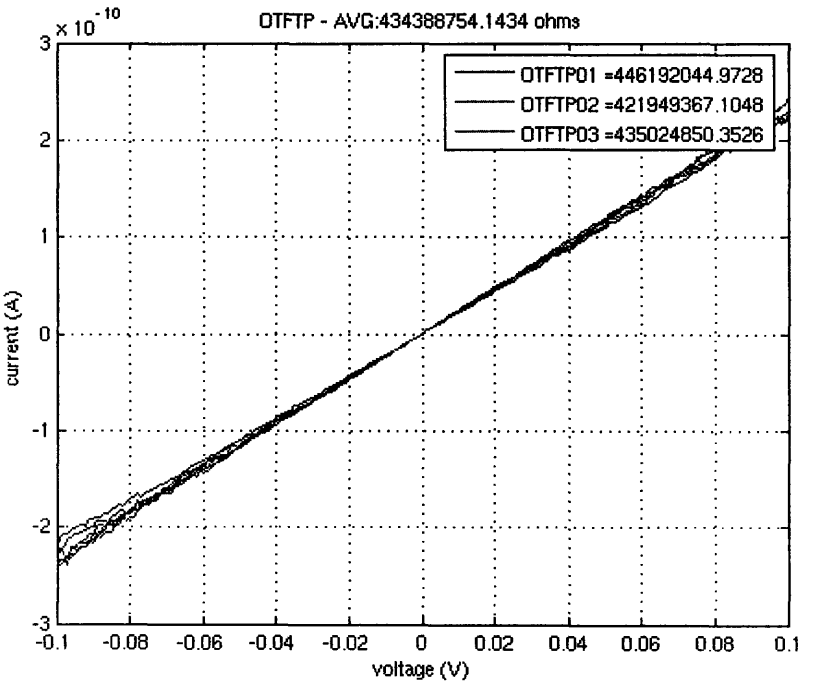

b)

Figure 10. a) Three I(V) curves for the OT:APDS-type film, **b)** Three I(V) curves for the OT:FTP-type film, both showing current fluctuations at higher applied voltages. The more significant fluctuations shown in **a)** are most likely the result of severe damage to the interdigitated electrodes.

Most of the I(V) curves taken for the eight types of nanoparticles tested were fairly linear, with occasional random fluctuations on certain electrodes, and with slight hysteresis in some of the films showing greater resistivity. The appearance of hysteresis in an IV curve most likely denotes the presence of an extra, unexpected mechanism of charge transfer in the sample. In the case of evaporated nanoparticle films, this mechanism would most likely come in the form of ionic conduction through solvent left on the surface, an effect of incomplete evaporation.

The conductance was calculated as the inverse of the resistance averaged from all of the IV curves plotted for each nanoparticle type. These values are given in **Table 2** and plotted in **Figures 11 and 12.**

Table 2. Average conductance for each type of nanoparticle film

Nanoparticle Type	Conductance (Siemens)
5,5'-dithiobis(2-nitrobenzoic acid) (DTNB)	4.23497E-07
4-aminophenyl disulfide (APDS)	4.94804E-07
4-flourothiophenol (FTP)	2.52092E-06
4-methylbenzenthiol (MBT)	8.14958E-10
octanethiol (OT)	2.11318E-10
1:1 OT:FTP	2.13344E-09
1:1 OT:APDS	2.82235E-07
1:1 OT:mercaptopropionic Acid (MPA)	8.26457E-09

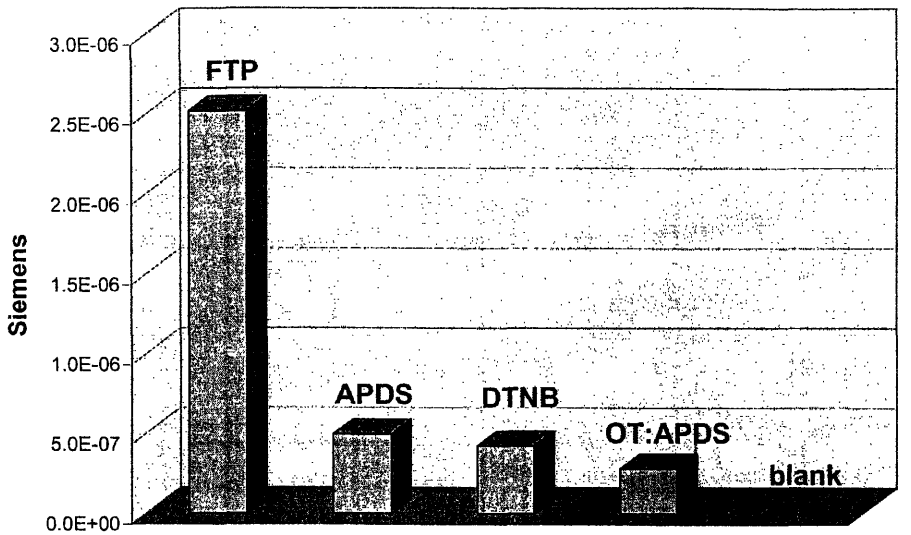

Figure 11. Average conductance (siemens) calculated for films composed of four nanoparticle types, as well as for an uncoated test substrate (blank). The four nanoparticle films shown in this figure displayed the highest conductance of the eight films studied. Some measurement issues remain to be solved, particularly those relating to the occasional occurrence of aberrational data points.

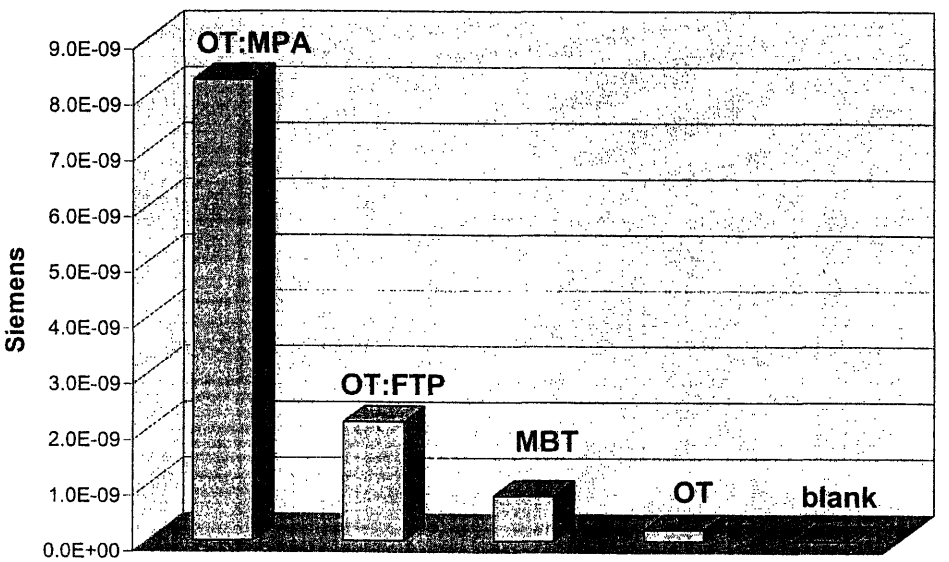

Figure 12. Average conductance (siemens) calculated for films composed of four nanoparticle types, as well as for an uncoated test substrate (blank). The four nanoparticle films shown in this figure displayed the lowest conductance of the eight films studied.

3.1 The Effects of Phenylated Ligands

The positive effect of pi-pi stacking on electronic conduction in the nanoparticle film is clearly demonstrated by the fact that the only four nanoparticle types to show significant conductance all contained phenylated ligands in their shells; of the four most conductive nanoparticle types, the top three were indeed entirely capped by phenylated ligands. The verity of this claim is somewhat undermined by the rank of the next two most conductive nanoparticle types – 1:1 OT:MPA and 1:1 OT:FTP. Since the later contained fluorothiophenol in the ligand shell, one might have expected a much higher conductance in this film than in the 1:1 OT:MPA film. However, in the case of rippled nanoparticles, the distance between particles seems not to be effect by interdigitation, but by the length of the longest ligand (which would be octanethiol in each of the heteroligand-capped nanoparticle types studied). This means that the model of charge transfer illustrated in **figure 3** no longer applies, as interdigitation and pi-pi stacking between conjugated ligands on adjacent particles cannot take place. Nanoparticles joined in this manner must rely on other mechanisms of charge transfer, electron hopping in particular, as the orbitals of their ligands do not overlap. The relative conductances calculated for the OT:MPA-type film and the OT:FTP-type film are then understandable as a function of the separation distance, or the combined length of the two ligand types. As 4-fluorothiophenol is longer than the mercaptopropionic acid molecule, the former nanoparticle type should and did demonstrate better conductance.

3.2 The Effects of Close-Packing

The possibly occluding presence of the octanethiol ligands in the shells of the heteroligand-capped nanoparticles must use the measurements taken on the 1:1 OT:APDS nanoparticle film as its closest basis for comparison. The film showed markedly higher conductance than the film comprised of 1:1 OT:FTP-capped nanoparticles. And while this slightly more complicated effect of the packing conformations taken on by the various ligand combinations might be difficult to draw out from the experimental data, the effect of packing on the conductance of the homoligand-capped nanoparticle films is dramatically apparent. The film comprised of nanoparticles capped with the ligand derived from 5,5'-dithiobis(2-nitrobenzoic acid) contains two very polar donor groups, and should have demonstrated the highest charge transfer capabilities among the nanoparticle types tested. The fact that the film comprised of nanoparticles capped with 4-fluorothiophenol registered an average conductance nearly an order of magnitude higher than the DTNB film attests to the tremendous effect of the extreme close packing ability in the nanoparticles of the former film, an ability that results from the small size of the fluorine atom end group. The bulky groups attached to the ligand derived from 5,5'-dithiobis(2-nitrobenzoic acid) seems to have partially prevented significant pi-pi stacking between the ligands, thus reducing the seemingly-high charge transfer capabilities of the ligand end groups.

3.3 The Effects of Donor/Acceptor Level

DeVries' STM study of electronic conduction through single nanoparticles concluded that "I(V) behavior primarily reflects energetic barrier to electron transfer

between molecular orbitals of ligands and Fermi level of gold" [25]. The current study again finds the electronic properties of the endgroups to be vitally important to determining the capacity for electronic conduction through nanoparticle films. The top conductor, a 4-fluorothiophenol-type film, benefits from the extreme electronegativity of the fluorine atom bonded to the four position of the phenyl group; the films composed of nanoparticles capped with 4-aminophenyl disulfide and 5,5' dithiobis (2-nitrobenzoic acid) also perform well due in large part to their highly polar end groups. When compared to the conductance of the FTP-type film, however, the lower conductances of the DTNB- and APDS-type films again show the importance of close-packing ability.

Figure 12 shows the four least conductive films to each be comprised of nanoparticles whose ligand shell compositions pose significant energy barriers. Both the OT- and OT:MPA-type film contains no phenylated ligands and thus cannot utilize pi-pi stacking to interdigitate, nor do the end groups of their ligands sufficiently displace charge to create significant conduction states. The MBT-type film could indeed be expected to engage in significant interdigitation given the presence of a phenyl group in the capping ligand. However, the methyl group, while small enough to insure close-packing throughout the ligand shell, suffers from an unfavorable Hammaker constant and thus cannot displace enough charge from the gold core to create a conductive state. The only film in this group containing a ligand with both a phenyl group and a strongly accepting endgroup is the OT:FTP-type film: to explain its poor behavior, we must examine the effects of ligand spacing and morphology as seen in the conductivity of films composed of heteroligand-capped nanoparticles.

3.4 Ligand Shell Phase Separation and Nanoparticle Morphology

The changes in ligand spacing and phase separation within the ligand shell predicted in heteroligand-capped nanoparticles seem to provide possible solutions to intra-shell packing problems posed by bulky end groups. Alternatively, the disruption of inter-shell pi-pi stacking would effectively isolate the charge-transfer mechanism predicted for heteroligand-type films, allowing for a comparison between the conductivity of films dependent upon electron-hopping for conductivity and more-heavily interdigitated films. This study sought to investigate these effects by comparing the electronic properties of homoligand-capped nanoparticle films to the properties of films composed of nanoparticles simultaneously capped with both phenylated ligands and non-phenylated, "spacer" ligands such as octanethiol. The poor performance of these heteroligand-capped nanoparticle films suggest that instead of merely providing extra space to ameliorate the effects of bulky end groups, these spacer ligands simply occluded adjacent phenylated ligands and disrupted interdigitation. The similar performance of the OT:MPA-type and OT:FTP-type films clearly indicates a disruption of the charge transfer mechanism detailed in the introduction to the current study. There is an intrinsic trade-off between conductivity and particle solubility which cannot be overcome.

4. Conclusions and Suggestions for Future Work

Upon measuring the I(V) characteristics of films comprised of phenylated ligand-capped nanoparticles and calculating average electronic conductance values based on

these measurements, the effect of these ligands on the electronic properties of the films was clearly shown. The three most conductive film-types all employed phenylated ligands with either highly polar or highly electronegative end groups, and as evidence of the effect of packing ability on nanoparticle capacity for interdigitation within cast films, the most conductive of these employed the ligand with the smallest end group. Furthermore, by comparing results from both homo- and heteroligand-capped nanoparticles, the conductance of interdigitated films was shown to be on average two orders of magnitude higher than the conductance of films reliant upon electron hopping as their chief charge transfer mechanism.

The findings of the current study could be clarified and supplemented in a number of ways. First, the lack of precision inherent in our drop-casting process was a constant cause of concern. Although measurements were taken on several pads for each round of tests in an effort to account for fluctuations in layer thickness, an improved coating process would improve the consistency of our data. Also, layer thickness characterization via elipsometry, atomic force microscopy or some other method would further normalize our measurements and hopefully provide the necessary dimensions for conductivity calculations.

The band structure of the ligand-capped nanoparticle system is extremely complex: in order to calculate it to any degree of accuracy, one would have to know the Hammaker constant of the phenylated ligand, the work function of the gold-thiol bond, the curvature and morphology of the nanoparticle surface, and the spacing of ligands within the ligand shell. While this is clearly beyond the scope of the current study, such a calculation would undoubtedly be useful for further study, particularly in comparisons of

electronic properties between ligand-capped nanoparticles and self-assembled monolayers of similar ligands. This information would also be useful in more precisely determining the effects of gating voltages and other applied fields on the conductance of nanoparticle films.

In order to more fully clarify the distinction between the charge transfer mechanisms proposed for homoligand- and heteroligand-type nanoparticle films, the electronic tests performed in the current study could easily be performed on a heated substrate. Increased temperatures should improve electron mobility and thus increase conductance through hopping mechanisms.

The results of further studies notwithstanding, thin-film charge transfer through interdigitation between conjugated ligands presents enticing possibilities for microeletronics fabrication technologies. By bridging the gap between organic semiconductors and metallic materials, conductive films comprised of phenylated ligand-capped nanoparticles promise to provide the properties demanded by today's microelectronic devices alongside the simplicity and functionality desired of the devices of tomorrow.

References

[1] A.L. Robinson, New Ways to Make Microcircuits Smaller, *Science*, New Series, **208** (1980) 4447, 1019-1022.

[2] *Epson*, Epson Inkjet Technology Used to Fabricate World's First Ultra-Thin Multilayer Circuit Board, http://www.epson.co.jp/e/newsroom/news_2004_11_01.htm. Accessed 23 May 2006.

[3] *RFID Journal*: "New Way to Print Ink Antennas," http://www.rfidjournal.com/article/articleview/618/1/1/. Accessed 23 May 2006.

[4] H. Dong , K.S. Moon, C.P. Wong, Molecular dynamics study on the coalescence of Cu nanoparticles and their deposition on the Cu substrate, *J. Elec. Mat.*, **33** (2004) 11, 1326-1330.

[5] M. Brust, Synthesis of thiol-derivatized gold nanoparticles in a 2-phase liquid-liquid system, *J. Am. Chem. Soc., Chem. Commun.*, **7** (1994), 801-802.

[6] S.Y. Kang, K.Kim, Comparative study of dodecanethiol-derivatized silver nanoparticles prepared in one-phase and two-phase systems, *Langmuir,* **14** (1998), 226-230.

[7] A.M. Jackson, J.W. Myerson, F. Stellacci, Spontaneous assembly of subnanometre-ordered domains in the ligand shell of monolayer-protected nanoparticles, *Nature Materials*, **3** (2004) 5, 330-336.

[8] A. Jackson, P. Jacob-Silva, F. Stellacci, in preparation.

[9] S. Hoeppener, A.S. Susha, A.L. Rogach, *et al.*, Guided self-assembly of Fe3O4

nanoparticles on chemically active surface templates generated by electro-oxidative nanolithography, *Current Nanoscience*, **2** (2006) 2, 135-141.

[10] F. Gutman, *Organic Semiconductors*, Wiley, New York, 1967.

[11] M. Meot-Ner, A.D. Adler, Interpretation of linear Hammett constant correlations in substituted ms-tetraphenylporphins, *J. Am. Chem. Soc.*, **13** (1972) 94, 4763-4764.

[12] L.S. Zhou, S.N. Park, B. Bai , *et al.*, Pentacene TFT driven AM OLED displays, *IEEE Electron. Device Letters* **26** (2005) 9, 640-642.

[13] M. Kitamura, T. Imada, Y. Arakawa, Organic light-emitting diodes driven by pentacene-based thin-film transistors, *App. Phys. Letters*, **83** (2003) 16, 3410-3412.

[14] M.G. Zheng, N. Vedova-Brook, K. Sohlberg, Application of a lumped-inertia technique to vibrational analysis of the torsional-twisting modes of low molecular weight polyphenylenes and polyethynylphenylenes, *J. Phys. Chem. A*, **108** (2004) 13, 2499-2507.

[15] R.V. Ball, G.M. Eckert, F.Gutmann, D.K.Y. Wong, Electrochemical Study of Amiodarone Charge-Transfer Complexes, *Anal. Chem.*, **66** (1994), 1198-1203.

[16] S.J. Wang, W.J. Oldham, R.A. Hudack, G.C. Bazan, Synthesis, morphology, and optical properties of tetrahedral oligo(phenylenevinylene) materials, *J. Am. Chem. Soc.*, **122** (200) 24, 5695-5709.

[17] A.P. Tyutnev, M.L. Keshtov, Y.F. Kundina, V.S. Saenko, E.D. Pozhidaev, Charge carrier transport in phenylated poly(naphthoylenebenzimidazole), *Polymer Science Series B*, **43** (2001) 7-8, 219-222.

[18] A.P. Tyutnev, M.L. Keshtov, V.S. Saenko, E.D. Pozhidaev, A.L. Rusanov, Y.I. Sezonov, Radiation-induced conductivity of phenylated polyphenylene, *Polymer Science Series B*, **43** (2001) 5-6, 137-139.

[19] L. Han, J. Luo, N.N. Kariuki, M.M. Maye, V.W. Jones, C.J. Zhong, Novel interparticle spatial properties of hydrogen-bonding mediated nanoparticle a ssembly, *Chemistry of Materials*, **15** (2003) 1, 29-37.

[20] O. Balmes, J.O. Bovin, J.O Malm, Self-healing and self-organized gold nanoparticle films at a water/organic solvent interface, *Journal of Nanoscience and Nanotechnology*, **6** (2006) 1, 130-134.

[21] C.Y. Yang, C.L. Li, C.J. Lu, A vapor selectivity study of microsensor arrays employing various functionalized ligand protected gold nanoclusters, *Analytica Chimica Acta*, **565** (2006) 1, 17-26.

[22] C. Sekar, C. Subramanian, Purification and characterization of buckminsterfullerene, nanotubes and their by-products, *Vacuum*, **47** (1995), 1289-1292.

[23] C.A. Waters et al, Purification of dodecanethiol derivatised gold nanoparticles, *J. Chem Soc., Chem. Commun.*, (2003), 540-541.

[24] S. Huang et al, Optical spectroscopic studies of dispersibility of gold nanoparticle solutions, *J. App. Phys.*, **92** (2002) 12, 7486-7490.

[25] G. Devries, J. Kuna, F. Stellacci, in preparation.